SANDIA REPORT SAND82-8210 · Unlimited Release
Printed February 1982

Thermal Convection Loop Corrosion Tests of 316SS and IN800 in Molten Nitrate Salts

R. W. Bradshaw

Prepared by
Sandia National Laboratories
Albuquerque, New Mexico 87185 and Livermore, California 94550
for the United States Department of Energy
under Contract DE-AC04-76DP00789

Issued by Sandia Laboratories, operated for the United States Department of Energy by Sandia Corporation.

SAND82-8210
Unlimited Release
Printed February 1982

THERMAL CONVECTION LOOP CORROSION TESTS OF 316SS AND IN800 IN MOLTEN NITRATE SALTS

R. W. Bradshaw
Exploratory Chemistry Division I
Sandia National Laboratories, Livermore

ABSTRACT

The corrosion behavior of Type 316 stainless steel and Incoloy 800 in molten $NaNO_3$-KNO_3 was studied using thermal convection loops which operated between the temperature limits, 630°C-350°C, for up to 4000 hours. Corrosion rates were approximately 1 mil/year (2.5×10^{-2} mm/year) at 600°C for 316SS but increased to about 4 mil/year at 630°C. Less extensive results are reported for IN800 but the corrosion rates appear to be similar to 316SS. Corrosion products consisted of the spinels, Fe_3O_4 and $Fe(Fe,Cr)_2O_4$, at temperatures below 600°C, although $NaFeO_2$ and $Fe(Fe,Cr)_2O_4$ were present at higher temperatures. In addition, internal oxide penetration was observed in IN800. Considerable spalling of surface scales was found at temperatures above 600°C and a mass balance was developed to estimate total corrosion rates from weight change and metallographic data. Chromium, but not iron or nickel, accumulated as a solute in the melt as a result of depletion from the alloys, but no thermal gradient mass transfer was detected.

CONTENTS

ILLUSTRATIONS

TABLES

THERMAL CONVECTION LOOP CORROSION TESTS OF 316SS AND IN800 IN MOLTEN NITRATE SALTS

Introduction

The molten salt mixture, $60NaNO_3$-$40KNO_3$ (w/o), is a prime candidate as a working fluid for central solar receiver systems [1,2]. The operating temperature range of a central receiver is expected to be 600°C-300°C and will involve thermal cycling at least daily. The choice of containment materials for such a system is based primarily upon corrosion resistance, mechanical properties and cost. Both 316SS and IN800 are being considered for this application because of their high temperature strength and general corrosion resistance.

Relatively little data is available concerning the corrosion behavior of these two alloys in molten alkali nitrates. Some results have been reported which indicate slow corrosion of 316SS and IN800 in nitrate melts at 595°C, resulting in weight gains of less than 2 mg/cm^2 after about 3000 hours, although corrosion product analyses were not reported [3]. However, a recent report concerning corrosion of IN800 undergoing creep showed more rapid corrosion [4]. Corrosion experiments conducted in a nitrate-nitrite salt mixture, $40NaNO_2$-$53KNO_3$-$7NaNO_3$ (w/o), have shown rapid weight loss of 316SS at 550°C with N_2 as a cover gas [5,6], but slow corrosion when air was in contact with the melt [7].

Since the available data are not adequate for assessing the reliability of 316SS and IN800 for containment of molten $NaNO_3$-KNO_3 mixtures, a study was undertaken to provide this information. This report describes the results of some preliminary corrosion experiments using thermal convection loops. Additional experiments are being conducted in both thermal convection loops and isothermal crucibles and will be reported subsequently. The purpose of this report is to quantify corrosion rates for an engineering evaluation of materials and to identify the corrosion products formed. Subsequent reports will attempt to develop a mechanistic understanding of corrosion behavior.

Experimental

Thermal convection loops were chosen as the experimental system since corrosion data can be acquired over a range of temperatures, matching that in a central solar receiver, in a single apparatus. In addition, the occurrence of mass transfer phenomena which are particular to non-isothermal flow systems can be identified. The design and operation of these loops has been described in detail elsewhere [8].

The maximum temperature in the loops was 630°C and the minimum was 350°C. The maximum was chosen to exceed that proposed for the operational system, 600°C, to provide an acceleration and over-test factor. Temperature variations were ± 10°C at a given location. The loops operated at steady-state conditions and thus the thermal cycles intrinsic to central solar receivers were not simulated in these tests.

The chemical compositions of the materials used to fabricate the loops and the removable test coupons are given in Table I. Coupons were polished with 180 grade SiC paper, vapor cleaned in trichlorethane and then rinsed in isopropanol. No surface preparation was used for the tubing. Inserted coupons were suspended from a sample tree at various locations to cover a range of temperatures. They were periodically removed for weighing and metallographic analysis. Specimens were quenched in air, rinsed in an ultrasonically in hot water, dried and weighed. At the termination of the experiment, the loops were sectioned for metallographic analysis.

In addition to examination of metallic coupons, the melt within the loop was periodically sampled and chemically analyzed. The loop was initially charged with a commercial mixture of 60 $NaNO_3$-40KNO_3 (w/o), (Partherm 430, Park Chemical Co., Detroit, MI). Concentrations of NO_2^-, CO_3^{-2} and oxide ions (as OH^-) were determined by titrimetric methods after dissolving quenched melt samples in water [9]. Metallic content was determined by atomic absorption spectroscopy. Additional salt was added only to compensate for periodic withdrawals of 10 gm samples for chemical analysis.

Results

The corrosion behavior of 316SS and IN800 is discussed separately in the sections which follow. The data presented concern weight changes as functions of time and temperature, identification and morphology of corrosion products and total extent of corrosion. Results for both inserted specimens and for the tubing from which the loops were fabricated are considered. Results are also presented which demonstrate that chromium is depleted from these alloys during contact with molten nitrates.

316SS: Weight Changes

The changes of weight with time of 316SS coupons which were immersed at various temperatures are plotted in Figures 1 and 2. The temperature range has been divided into those coupons at temperatures at 600°C or less and those at higher temperatures. This division was chosen according to the maximum expected operating temperature as well as the different behavior observed. Note that data for 600°C appears on both graphs to facilitate comparison.

At temperatures limited by 600°C, Figure 1, the weight changes observed did not greatly exceed 2 mg/cm^2 after about 4000 hours of immersion. The weight changes were relatively insensitive to temperature in this range and the largest weight changes were actually recorded at the lowest temperature,

510°C. The weight gains tend toward asymptotic values rather than exhibiting negative slopes after long times, as previously noted for 304SS in nitrate melts [10].

At temperatures greater than 610°C, the weight change curves appear distinctly different, see Figure 2, since weight losses occurred instead of gains. The size of the weight losses increased as temperature increased and the peak in the positive weight gain portion of the curve occurred at shorter times. Since a weight loss of 1 mg/cm^2 corresponds to approximately 5 microns of metal thickness it is evident that several mils (1 mil = 25.4 microns) of metal loss occurs after a few thousand hours.

Although weight change measurements provide a convenient figure-of-merit for evaluating corrosion behavior, the interpretation of such data is not straightforward in this situation. These data will be discussed fully in a subsequent section. Results concerning the extent of corrosion and identification of corrosion products are reported in the next several sections.

316SS: Corrosion Chemistry; < 600°C

Corrosion of 316SS by molten $NaNO_3$-KNO_3 formed multiple product phases which were primarily iron-rich oxides. The photomicrograph in Figure 3 depicts typical oxidation behavior of polished coupons at temperatures less than 600°C, insofar as types of oxidation products are concerned. The corrosion products consisted of three distinct phases, whose semi-quantitative analysis by x-ray energy dispersive spectroscopy (EDS) are shown. At the outer (salt-contacting) surface, iron was the primary metallic constituent of the oxide as demonstrated by the spectrum corresponding to area A. This layer was identified as Fe_3O_4, magnetite, by x-ray diffraction analysis. Beneath A, a thinner oxide layer, B, was formed which was still primarily iron but contained some Cr and Ni. The EDS spectra and X-ray diffraction patterns are consistent with a spinel-type oxide, $Fe(Fe,Cr)_2O_4$, where Fe:Cr ratio is greater than 2 [11]. Beneath layer B, an irregular front of oxidation penetrated into the metal and, as shown by the corresponding EDS spectrum, region C contains the metallic elements in about the same proportions as the original alloy. Examination of tubing segments removed from unheated sections of the loop, where temperatures were 600°C or less, revealed similar oxidation products.

316SS: Corrosion Chemistry; 600 - 630°C

The weight change data presented in Figure 2 demonstrated that increasingly rapid deterioration of 316SS occured at temperatures above 600°C and up to 630°C, the highest temperature studied. Metallographic and chemical analysis of the corrosion products formed in this temperature range provides a better understanding of the corrosion process. A photomicrograph of an oxide scale formed on a 316SS coupon after 4430 hours at 630°C is presented in Figure 4. The outer layer comprised the majority of the oxidation products, as at lower temperatures, although the chemistry of the scale changed. The outer layer was identified as sodium ferrate, $NaFeO_2$, by x-ray diffraction. Beneath this layer, the mixed spinel layer, $Fe(Fe,Cr)_2O_4$, was identified and, adjacent to the metal, an irregular internal oxide penetration zone containing all the metallic elements.

316SS: Temperature Dependence of Corrosion Rate

The extent of corrosion, as given by the sum of scaling thickness and depth of penetration, of 316SS coupons after 4430 hours is plotted in Figure 5 as a function of reciprocal temperature. The scaling thickness and penetration depth at each temperature were determined by averaging a number of measurements made directly on photomicrographs of cross-sectioned coupons. The trend of the data strongly suggest that two different processes control the corrosion process at different temperatures. The temperature dependence of the overall oxidation process was more pronounced at higher temperatures than at lower temperatures. As indicated by the solid line on Figure 5, the points corresponding to the three highest temperatures were consistent with an activation energy of 35 kcal. The limiting value for the activation energy at the lower temperatures, as indicated by the dashed line, was only 4.5 kcal.

IN800: General Observations of Corrosion Behavior

The data obtained from the IN800 loop were limited because accidental overheating of the hot leg, after 4000 hours, damaged the inserted coupons, as well as that leg. However, the data available do permit a preliminary evaluation of IN800 and comparisons with 316SS.

The corrosion behavior of IN800 at the highest temperature studied is illustrated by the weight change curves plotted in Figure 6, which corresponds to temperatures of 600°C, 615°C and 625°C. The general trends of weight changes in IN800 resembles those of 316SS. At 600°C, the net weight change was relatively small and became nearly constant after several thousand hours. At higher temperatures, weight changes decreased with time and became more negative as the temperature increased. Although the data concerning IN800 were not obtained over as long a period of time as 316SS, IN800 appears to lose weight less rapidly at relatively high temperatures.

Investigation of corrosion morphologies of IN800 was restricted to sections of tubing obtained from the unheated vertical legs of the loop because accidental overheating distorted the results from other areas. Sections of tubing were removed from regions at several temperatures between 530°C and 390°C and examined metallographically. The corrosion morphology typical of all sections is shown in Figure 7, corresponding to 530°C. The surface oxide layer, A, was an iron oxide, probably Fe_3O_4. Beneath this layer, another continuous layer formed which appeared to be a mixed spinel oxide, $Fe(Fe,Cr)_2O_4$, as described previously for 316SS. Sub-surface phases were discontinuous, consisting of a chromium-rich oxide phase, C, and metallic regions, D, which were essentially pure nickel. Adjacent to the metal, a dispersed mixture of oxidized and unreacted material was observed, E, where Fe, Cr and Ni were present in the same proportions as in the alloy.

Despite the relatively low temperature, the depth of affected metal was considerably more than that reported in Figure 5 for 316SS. Much of the additional oxidation of IN800 was due to internal oxide penetration, as described above, which was relatively minor in 316SS. Measurements of the total affected depth, the sum of scaling and penetration, are plotted in

Figure 8 versus reciprocal temperature. The temperature sensitivity of the overall corrosion process in IN800 tube sections appears to be rather low. A value of 7.5 Kcal was calculated for the activation energy of the straight line shown in Figure 8. This value is comparable to that determined for 316SS at the lower temperatures.

Mass Transfer Effects

Mass transfer effects were evaluated by determining if alloying constituents were soluble in the melt and by examining the coldest sections of the loops for deposits caused by precipitation of insoluble species. Atomic absorption spectroscopy of salt samples periodically withdrawn from both loops indicated the presence of chromium. Only a few ppm of iron and nickel were detected, which probably arise from background effects. The concentration of Cr in each loop, in ppm by weight, is plotted in Figure 9 versus time. The data in Figure 9 do not necessarily indicate relative Cr depletion rates for each alloy since the timing of coupon insertions and the temperature distributions were not the same in each loop. However, in each loop the Cr concentration increased with time. At times greater than 3000 hours, the rate of increase appears to slow in 316SS. In neither loop was a steady-state value of Cr concentration reached, which implies that thermal gradient mass transfer of Cr did not occur or that the deposition rate of Cr is much less than depletion rate.

Evidence that the deposition rate of Cr was low was provided by the fact that coupons in the coldest part of the loop experienced a weight gain of less than 1 mg/cm^2 , which was primarily due to oxidation. The absence of thermal gradient mass transport of chromium was also indicated by the absence of Cr-containing deposits on sections of tubing removed from the lower crossleg. An examination by Auger electron spectroscopy indicated only a very thin film containing primarily Mg, Ca, Si, O and C which was sputtered away quite easily. The elements in the deposit derive from the impurities present in the salt and their interaction with oxygen from the salt and CO_2 from the atmosphere. The deposit appears to be a mixture of alkaline earth silicates and carbonates which are insoluble in the melt. Deposits of this type appear to present no operational problems since they are limited by the low initial concentrations of these elements in the salt.

The identity of the Cr species in the melt have not been determined. However, due to the oxidizing nature of molten nitrates, it is likely that it is some type of chromate, either the Cr^{+3} oxidation state, CrO_4^{-5} or CrO_3^{-3}, or the Cr^{+6} oxidation state, CrO_4^{-2} or $Cr_2O_7^{-2}$. It has been reported that the trivalent form was found to oxidize to the hexavalent form, CrO_4^{-2}, at 250°C [13]. Published binary phase diagrams for the nitrate-chromate and nitrate-dichromate systems indicate at least several weight percent (> 10^4 ppm) solubility of Cr at temepratures as low as 350°C [14]. Assuming that Cr is oxidized to its highest valence in the melt, the observed absence of thermal gradient mass transport is quite reasonable.

Melt Chemistry

The results of chemical analyses for nitrite and carbonate ions appear in Table II. No oxide ions were detected by the analytical technique which was sensitive to 8×10^{-4} w/o [9]. The NO_2^- concentration in each loop was in the range of 7-8 w/o during the early part of the tests, which is slightly less than the equilibrium value of 8.2 w/o, which was calculated for the reaction, $NO_3^- = NO_2^- + 1/2\ O_2$, in air at 630°C using a value of 8.8×10^{-2} $atm^{1/2}$ for the equilibrium constant [9]. Variations in NO_2^- concentration may arise from temperature fluctuations during the test or chemical factors such as other decomposition reactions or oxide ion reactions related to chromate or carbonate concentrations.

The concentration of CO_3^{-2} appeared to increase linearly with time as CO_2 was absorbed from the atmosphere. The differences between the two loops is probably attributable to different amounts of CO_3^{-2} impurities in the initial salt charge to each loop.

Discussion

Total Metal Loss

The net weight change of the test coupons is the sum of weight gained by oxidation processes minus weight loss by chromium depletion and spalling of oxide layers. However, total metal loss, which is the reduction of load bearing metal section thickness, is the sum of metal consumption by oxidation and losses due to Cr depletion. Metal loss is not directly proportional to net weight change when several processes make offsetting contributions, as in the present case. Net weight change data underestimate total metal loss and therefore, supplementary measurements such as metallographic analysis, as used here, weight loss after descaling or direct measurements of thickness are needed to obtain an accurate assessment of corrosion rates.

Metal loss due to oxidation can be calculated from measurements of the thickness of each oxidation product layer, given the densities of the alloy and the oxidation products. A simple mass balance may be used, so $L_m = W_i\ L_i\ (\rho_i/\rho_m)$, where L_m = thickness of metal consumed, W_i = weight fraction of metal in i^{th} oxidation product, L_i = thickness of oxidation product layer, ρ_i = density of product and ρ_m = density of alloy. The contribution of all the products are then summed. The density values are as follows: alloy, 8 gm/cm^3 [15], Fe_3O_4, 5.7 gm/cm^3, $NaFeO_2$, 4.1 gm/cm^3[16]. The weight fractions are 0.724 for Fe_3O_4 and 0.505 for $NaFeO_2$. A weight gain of 1 mg/cm^2 resulting from formation of Fe_3O_4 corresponds to formation of 6.4 microns of scale and 3.7 microns of metal consumption, while a similar weight gain due to $NaFeO_2$ formation corresponds to 4.9 microns of scaling and 1.5 microns of metal consumption.

As a practical matter, it would require considerable effort to identify and measure each scale layer when several corrosion products form, as at products of 316SS are relatively simple. Assuming both Fe_3O_4 and $Fe\ (Fe,Cr)_2O_4$ have the same density, the metal loss rate of 316SS due to

scaling was calculated using the scale thickness data in Figure 5. The results are given in Table 3 where a linear extrapolation was used to obtain annual rates from data at 4430 hours. As shown, the value at 600°C for isothermal immersion is 0.8 mil/year.

The extent of chromium depletion cannot be determined directly from measurements of scaling and weight changes since spallation introduces a large uncertainty in the mass balance. However, a rough estimate of Cr depletion can be obtained from the amount of Cr dissolved in the salt. Assume that only the portion of the loops at temperatures above 600°C was depleted, which obviously yields an upper bound on the true value of Cr loss in that area. Since each loop contained 1.3 Kg of salt and about 420 cm^2 of tube and coupon surface experienced temperatures above 600°C, the estimates of Cr depletion at the end of each test are 2.2 mg/cm^2 for 316SS and 1.8 mg/cm^2 for IN800 can be calculated from the Cr concentration data in Figure 9. Since a loss of 1 mg/cm^2 corresponds to total depletion of a zone 6 microns thick in an alloy containing 20 w/o Cr, the estimates given above correspond to depletion zones about 12 microns (0.5 mil) thick.

The amount of spalling can be estimated from data on weight changes and scaling. As an example consider 316SS at 630°C where spalling was evident visually. The net weight change in this case was -13.5 mg/cm^2 (Fig. 2) and 47 microns of scale were formed (Fig. 5). This amount of scaling would result in a weight gain of about 10 mg/cm^2, since it is a mixture of $NaFeO_2$, spinel and internal oxidation. Therefore, about 23.5 mg/cm^2 were lost due to Cr depletion and oxide spalling. Only a minor portion, perhaps 4-5 mg/cm^2, of this net weight loss can be attributed to Cr depletion, assuming twice the average value calculated above. Therefore, the major loss mechanism was spalling, which was consistent with visual observations of the coupons. At temperatures below 600°C, the scales appeared to be adherent.

Oxidation Mechanisms

An important feature of the corrosion process of the two alloys studied was that the oxide scales formed were either M_3O_4-type spinels or $NaFeO_2$. The formation of the latter oxide at high temperatures is consistent with calculations of thermodynamic stability in nitrate melts [18]. Typically, alloys having Cr contents as large as IN800 or 316SS form Cr_2O_3 surface layers in oxidizing environments [20], however, the solubility of Cr in the melt prevented Cr_2O_3 from forming. Therefore, corrosion protection must be provided by inherently less protective spinels, such as Fe_3O_4 or the mixed oxide, Fe $(Fe,Cr)_2O_4$, in the temperature range specified for receiver operation.

The kinetics and mechanisms of alloy oxidation in molten nitrates are obviously too complicated to be determined solely from the data reported for these thermal convection loop tests. A study with this goal is being conducted using isothermal immersion tests where more frequent microstructural analysis and measurements of Cr depletion as a function of time and temperature are possible. In addition, marker experiments are being attempted to delineate the mass transport processes occurring during oxidation. At this time, however, some speculation concerning the corrosion phenomena observed so far seems appropriate.

The activation energies calculated for scale growth on 316SS (see Figure 5) indicate a transition in the rate-controlling process as temperature increases. This transition occurs in the temperature range, 550°C to 600°C, where $NaFeO_2$ replaces Fe_3O_4 as the surface oxide phase. At temperatures below this range, the activation energy was about 5-10 kcal, a value which is representative of liquid phase diffusion in molten nitrates [21]. This suggests that corrosion in the lower temperature range may be controlled by diffusion in salt-filled microcracks in corrosion product layers [22]. Such cracks or microporosity would not necessarily be detectable in metallographic cross-sections. At temperatures above 600°C, the activation energy was about 35 kcal, which is typical of solid state diffusion processes [20]. At high temperatures then, it is likely that diffusion in one or more solid product layers controls the corrosion rate.

The morphology of the multiple corrosion product layers observed appears to result from bi-directional transport processes. Microscopic examination of cross-sectioned coupons suggests that the original metal surface coincides with either the Fe_3O_4/mixed spinel interface or the $NaFeO_2$/mixed spinel interface, according to the temperature. Since the mixed spinel layer contains Fe, Cr and Ni, it is probable that this layer is formed by ingress of oxide ions from the salt, while outward migration of iron results in formation of surface layers of Fe_3O_4 or $NaFeO_2$.

Interpreting Cr depletion phenomena is a very uncertain exercise since it is not possible to obtain rate data or activation energies from thermal convection loop tests. However, if the discussion is limited to the temperature regime where Fe_3O_4 is the surface oxide layer, the following comments apply. The diffusivity of Cr in Fe_3O_4 has been reported to be 10^3 less than that of Fe [17]. Therefore, if Cr depletion were controlled by diffusion in a compact layer of Fe_3O_4 a large gradient in Cr concentration should be established across the Fe_3O_4 layer. However virtually no Cr can be detected in the Fe_3O_4 layer by EDS. Similar results were also observed in a 304SS loop where Fe_3O_4 and mixed spinel were also the corrosion products [10]. These observations suggest that the Fe_3O_4 layer is not compact and that Cr diffusion in this layer occurs via salt-filled microcracks or microporosity. If solid-state diffusion controls Cr depletion, either the mixed spinel layer or the alloy matrix could be the controlling regions, but not the Fe_3O_4 layer. Future measurements of the activation energy of Cr depletion kinetics should determine which process occurs.

Practical Implications

The results which have been presented in this report show that the maximum metal loss rate expected at 600°C, which corresponds to the maximum wall temperature in the receiver during normal operation, is about 1 mil/year for 316SS. Such a corrosion rate is consistent with operating lifetimes of 30 years, assuming that stress and fatigue conditions do not drastically change corrosion behavior. However, these results must also be considered in view of operating practices expected in central solar receivers to judge the suitability of materials with confidence. Some relevant factors which are briefly discussed here are thermal cycling, surface finish, nitrite concentration and breathing mode opertion.

The corrosion tests were conducted using constant temperatures during the test period. Since thermal cycling is inherent in receiver operation, however, corrosion rates will tend to increase due to spalling of surface oxide layers. The scales formed on 316SS and IN800 were generally adherent except at temperatures approaching 630°C. In addition, the adherence of scales formed on the inner diameter of tubing may benefit from the compressive stresses produced by scale growth which tend to enhance scale-metal contact. The effect of thermal cycling can only be reliably determined by experiment.

The effect of surface finish was studied briefly by comparing polished coupons with as-received tubing, rather than evaluating a number of typical treatments such as grit blasting, honing or electropolishing. The results indicated relatively little difference for 316SS, but IN800 tubing demonstrated considerable internal oxidation of unpolished tubing. Approximately 2 mils/year of metal loss was observed for IN800 at 540°C, the highest temperature at which reliable data was obtained. Additional experiments are being conducted to obtain data on IN800 over the entire temperature range of interest and to examine the behavior of polished coupons.

The concentration of nitrite ion, produced by the reaction, $NO_3^- = NO_2^- + 1/2O_2$, increases with increasing temperature [9]. The NO_2^- concentration in these tests, which was uniform throughout the loops, exceeded the value expected when operating within the specified temperature range, e.g. 3 w/o at 600°C versus 7 w/o at 630°C. Although the effect of NO_2^- on corrosion has not been established conclusively, related studies suggest that corrosion rates will increase as NO_2^- concentration increases [5,6]. In that case, the corrosion rates reported here may be over-estimates.

It appears that operating the loops in breathing mode, where CO_2 and H_2O can be absorbed from the atmosphere, does not create any significant corrosion problems. Since CO_2 is a weak acid in the Lux-Flood system, it will cause only small changes in oxide ion concentration in the melt. In addition, the absorption of CO_2 will tend to neutralize basic species which result from H_2O absorption and may thereby inhibit the accelerated corrosion caused by basic species [19].

Lastly, the initial selection of alloys for molten nitrate containment has largely concerned those alloys which perform well at similar temperatures in other oxidizing environments. However, since it was found that Fe-Cr spinels were formed rather than Cr_2O_3, in molten nitrates, less Cr may be required for corrosion resistance than the amount in IN800 and 316SS (20-18 w/o). Such a reduction would permit the use of less costly alloys.

Conclusions

Corrosion tests conducted in molten $NaNO_3$-KNO_3 demonstrated that the metal loss rate expected for 316SS at 600°C (1110°F) was 1 mil/year under isothermal conditions. Although limited results were obtained for IN800, a similar corrosion rate is expected based on the weight change data collected. Both alloys experienced chromium depletion due to the solubility of chromium

in the salt, but this phenomenon was neither the major factor in metal loss nor does it cause thermal gradient mass transport of chromium. Both alloys appear to be suitable for long-term applications in molten salt central solar receivers on the basis of these tests.

At temperatures above 600°C, the corrosion rate increased significantly with temperature and neither alloy was suitable for long-term service in receiver tubes. At 630°C, the maximum experimental temperature, the metal loss rate of 316SS was 4 mils/year. Above about 600°C, the primary corrosion product shifted from Fe_3O_4 to $NaFeO_2$ and the surface layers tended to spall, leading to linear weight loss kinetics.

Surface finish had a significant effect on both the rate and type of corrosion products formed on IN800. Tubing used in the as-received condition experienced considerable internal oxide penetration in addition to surface scaling.

TABLE I

CHEMICAL COMPOSITIONS OF ALLOYS

	Fe	Ni	Cr	Mn	C	others
316SS*	Balance	10-14	16-18	1.5 max	0.08 max	2-3 Mo
IN800**						
Tube	43.4	32.8	21.2	1.02	0.04	0.52 Al, 0.47 Ti, 0.43 Cu
Coupons	45.9	31.0	20.7	0.86	0.02	0.44 Al, 0.45 Ti, 0.57 Cu

*Nominal specifications.

**Chemical analysis.

TABLE II

NITRITE AND CARBONATE CONCENTRATIONS
DURING OPERATION OF THE LOOPS

316SS Loop	Time (Hrs)				
	1073	1553	3258	4795	5511
NO_2^- (w/o)	7.9	7.1	5.3	5.5	4.5
CO_3^{2-} (w/o)	1.0	-	1.15	-	1.25

IN800 Loop	Time (Hrs)		
	1845	2688	4148
NO_2^- (w/o)	7.0	5.8	7.1
CO_3^{2-} (w/o)	0.55	0.89	0.95

TABLE III

METAL LOSS RATE DUE TO SCALING OF 316SS

Temperature (°C)	Scale Thickness (microns, 4430 hours)	Metal Loss Rate (mils/year)
600	20	0.80
575	14	0.56
540	10	0.40
510	9	0.36

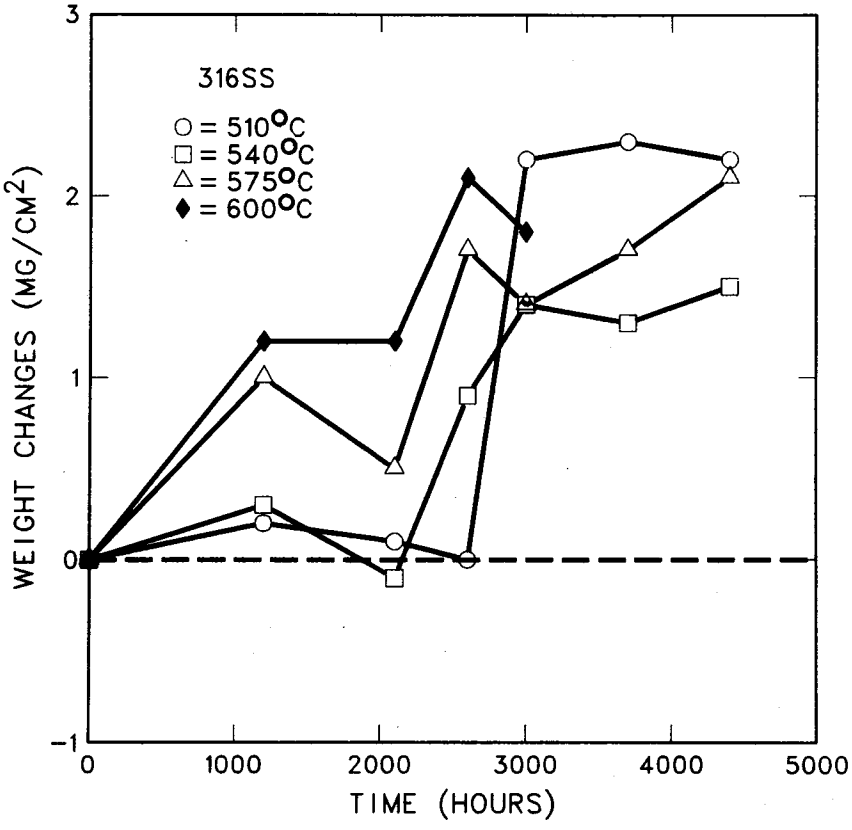

Figure 1. Weight Changes vs. Time for 316SS at Temperatures between 510°C and 600°C.

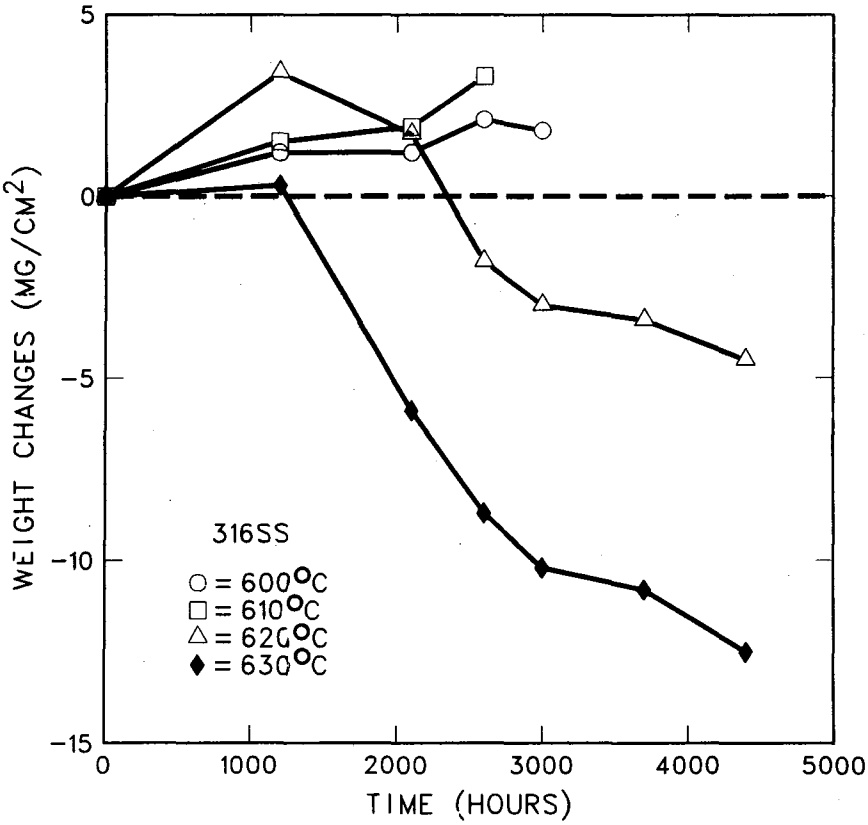

Figure 2. Weight Changes vs. Time for 316SS at Temperatures between 600°C and 630°C.

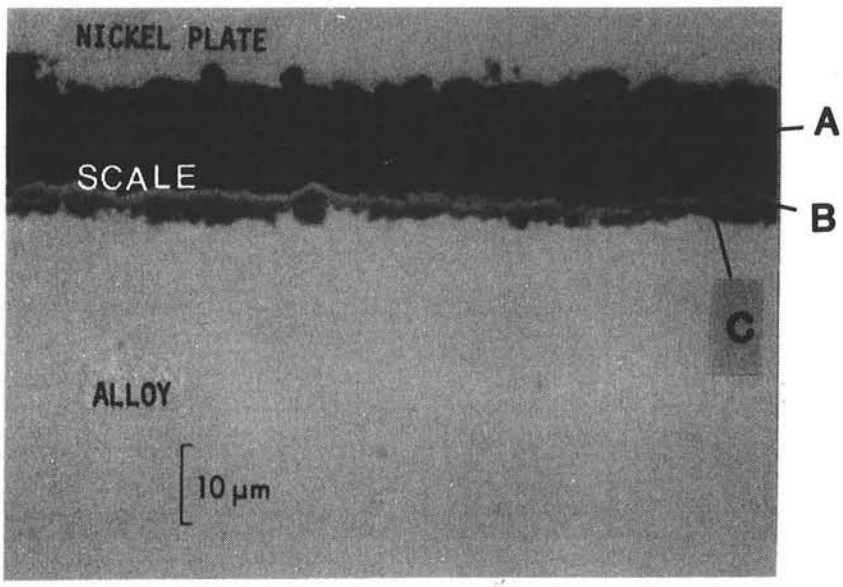

	EDS Analysis (counts)			
Location	Fe	Cr	Ni	Mo
A	5482	--	218	--
B	6142	969	--	--
C	6256	1403	1496	532
Alloy	6906	2847	848	417

Figure 3. Oxide Scale Composition on 316SS after 4430 Hours at 575°C.

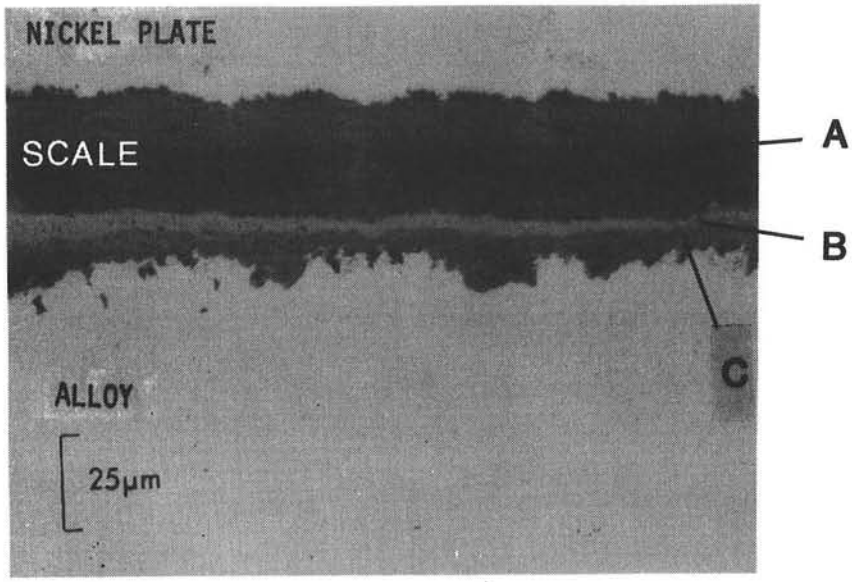

A $NaFeO_2$
B $Fe(Fe, Cr)_2O_4$
C Fe, Ni, Cr Oxide

Figure 4. Oxide Scale Microstructure on 316SS after 4430 Hours at 630°C.

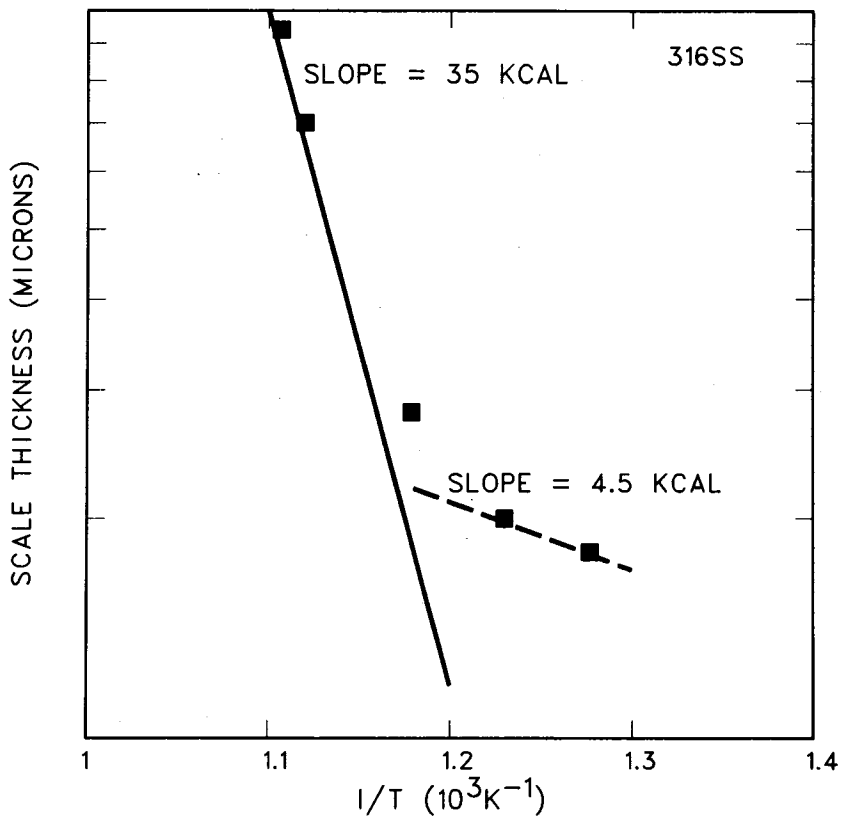

Figure 5. Arrhenius Plot of Total Scale Thickness on 316SS after 4430 Hours in Molten $NaNO_3$-KNO_3.

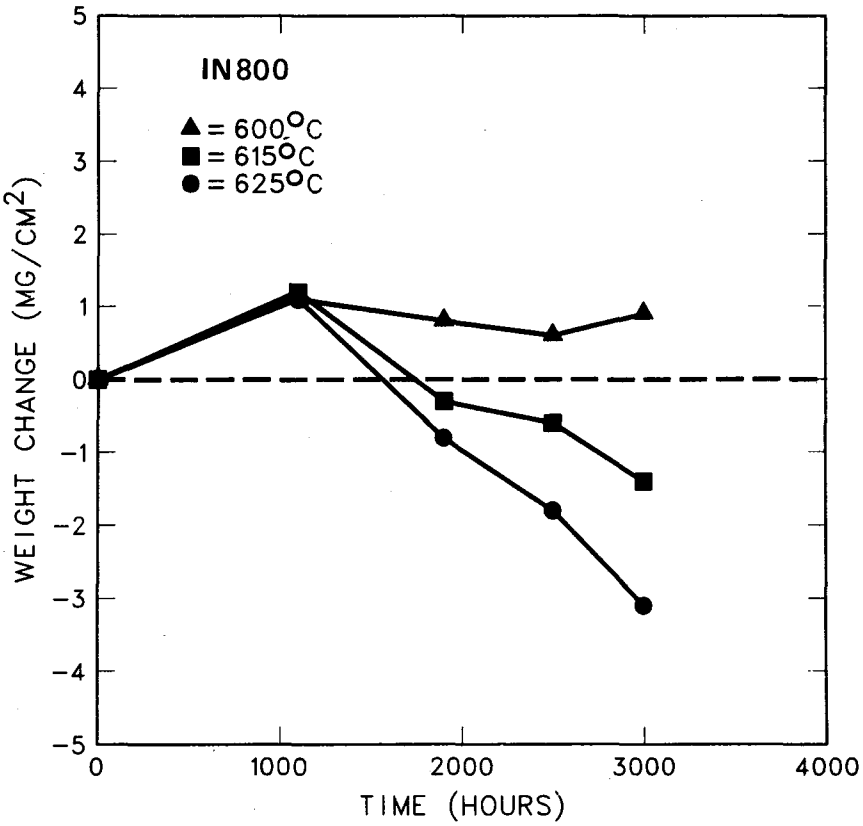

Figure 6. Weight Changes vs. Time for IN800 at Several Temperatures.

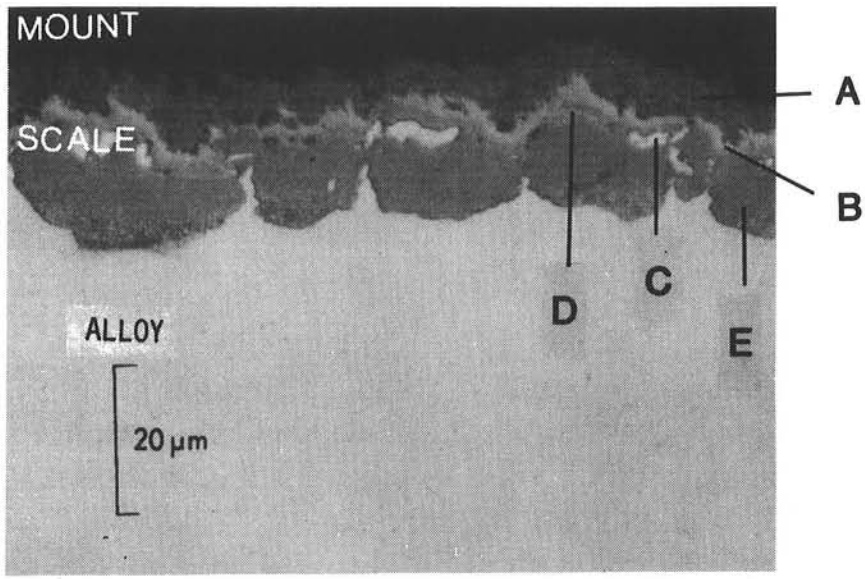

A	Fe_3O_4
B	$Fe(Fe, Cr)_2O_4$
C	Ni (metallic)
D	Oxide; Cr > Ni, Fe
E	Oxide; Fe > Ni > Cr

Figure 7. Corrosion Product Microstructure on Unpolished IN800 Tubing after 4148 Hours at 540°C.

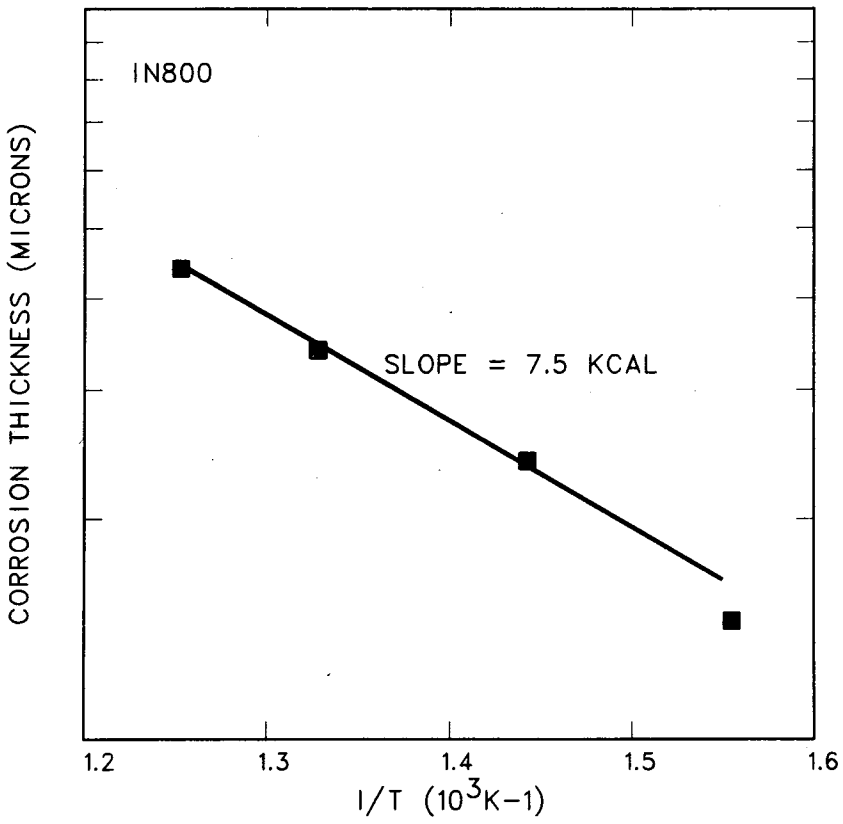

Figure 8. Arrhenius Plot of Scaling and Internal Oxide Penetration Depth for IN800 Tubing.

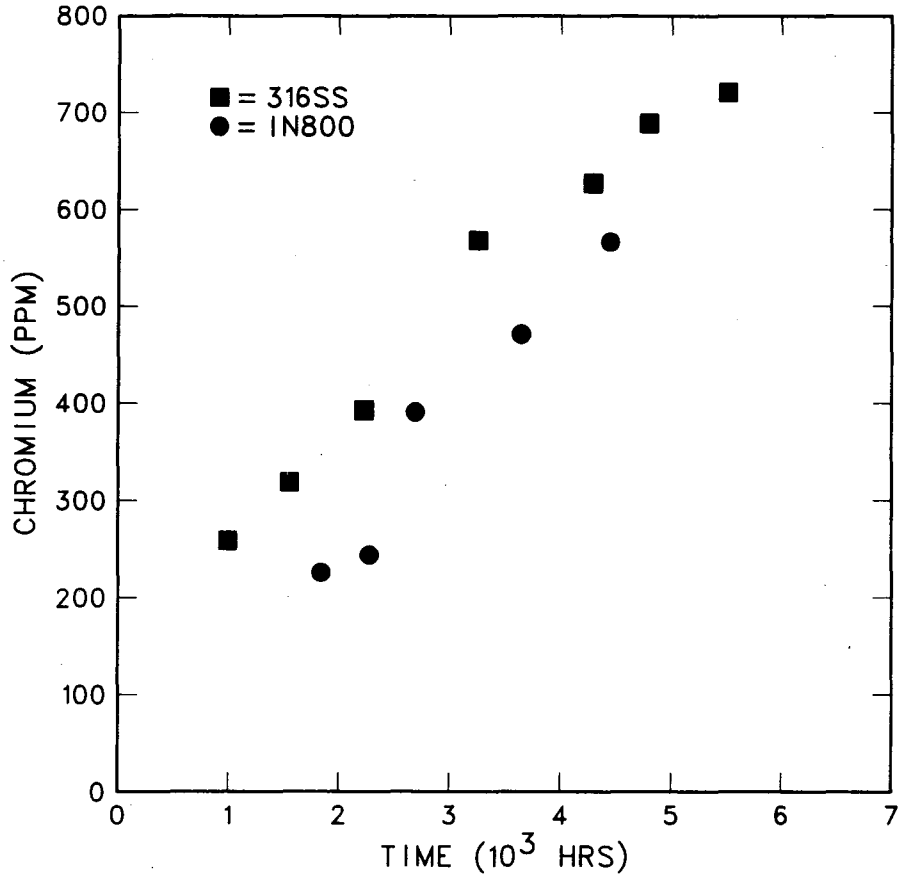

Figure 9. Concentration of Soluble Chromium in Each Loop as a Function of Time.

REFERENCES

1. A. F. Hildebrandt and S. Dasgupta, J. Solar Energy Eng., 102, 91 (1980).

2. R. W. Carling, et al., "Molten Nitrate Salt Technology Development Status Report," Sandia National Laboratories, Report SAND80-8052, 1981.

3. T. R. Tracey, "Conceptual Design of Advanced Central Receiver Power Systems," Martin Marietta Corporation Report, Contract EG-77-C-03-1724, 1978.

4. S. H. Goods, "Creep and Corrosion Characteristics of Incoloy Alloy 800 in Molten Nitrate Salts," Sandia National Laboratories, Report SAND81-8665, 1981.

5. J. R. Keiser, J. H. DeVan and E. J. Lawrence, J. Nucl. Mater., 85, 275 (1979).

6. P. Spiteri, "Corrosion of Different Steels in Na-K-Nitrate-Nitrite Mixture (HTS)," Molten Nitrate Salt Technology Workshop, Dublin, CA, Oct. 30, 1980.

7. C. M. Kramer, W. H. Smyrl and W. B. Estill, J. Mater. Energy Sys., 1(4), 59 (1980).

8. W. S. Winters, R. W. Bradshaw and F. W. Hart, "Design and Operation of Thermal Convection Loops for Corrosion Testing in Molten $NaNO_3$-KNO_3," Sandia National Laboratories, Report SAND80-8212, 1980.

9. D. A. Nissen, "Chemistry of the Binary $NaNO_3$-KNO_3 System," Sandia National Laboratories, Report SAND81-8006, 1981.

10. R. W. Bradshaw, "Corrosion of 304SS by Molten $NaNO_3$-KNO_3 in a Thermal Convection Loop," Sandia National Laboratories, Report SAND80-8856, 1980.

11. B. J. Isherwood and T. F. J. Quinn, Brit. J. Appl. Phys., 18, 717 (1967).

12. W. H. Smyrl, "Corrosion in Molten Salts Used for Solar Thermal Storage Applications," Sandia National Laboratories, Report SAND79-0246C, 1979.

13. B. J. Brough, D. H. Kerridge and S. A. Tariq, Inorg. Chem. Acta, 1, 267 (1967).

14. "Phase Diagrams for Ceramists," E. M. Levin, C. R. Robbins and H. F. McMurdie, Amer. Ceram. Soc., 1969 Supplement.

15. N.A.C.E. Corrosion Engineer's Reference Book, R. S. Treseder, ed., N.A.C.E., 1980.

16. Handbook of Chemistry and Physics, R. C. Weast, ed., CRC Press, 61st edition, 1980.

17. R. Dieckmann et al., Ber. Bunsenges Phys. Chem., 82, 778 (1978).

18. A. S. Nagelberg and R. W. Mar, "Thermochemistry of Nitrate Salts", Sandia National Laboratories, Report SAND81-8879, 1982.

19. Y. I. Sorokin and K. L. Tseitlin, Khim Prom., 41(1), 64 (1965).

20. S. Mrowec and T. Werber, Gas Corrosion of Metals, NBS translation, TT-76-54038, 1978, p. 333 ff.

21. H. Bloom, The Chemistry of Molten Salts, Benjamin, 1967, p. 98.

22. A. W. D. Hills, Heterogeneous Kinetics at Elevated Temperatures, G. R. Belton and W. L. Worrell, editors, Plenum, 1979, p. 449.

ACKNOWLEDGMENTS

The author gratefully acknowledges the efforts of the people listed below for their significant contribution to this study.

D. R. Boehme	X-ray diffraction
W. M. Clift	Auger spectroscopy
F. W. Hart	Apparatus design and fabrication
C. W. Karfs	Electron microscopy
D. E. Meeker	Chemical analysis
S. P. Orth	Electron microscopy

UNLIMITED RELEASE

INITIAL DISTRIBUTION

U. S. Department of Energy (5)
Division of Solar Thermal Technology
James Forrestal Building
1000 Independence Avenue S.W.
Washington, DC 20585
Attn: W. W. Auer
G. W. Braun
K. T. Cherian
C. B. McFarland
J. E. Rannels

U. S. Department of Energy
Division of Thermal and Chemical Energy Storage Systems
James Forrestal Building
1000 Independence Avenue, S.W.
Washington, DC 20585
Attn: J. H. Swisher

U. S. Department of Energy (2)
San Francisco Operations Office
Division of Solar Technology
1333 Broadway
Oakland, CA 94612
Attn: S. D. Elliott
R. W. Hughey

Aerospace Corporation
P.O. Box 92957
Los Angeles, CA 90009
Attn: P. Mathur

Arizona Public Service Co.
P.O. Box 21666
Phoenix, AZ 85036
Attn: E. Weber

Babcock & Wilcox
20 S. Van Buren Avenue
Barberton, OH 44203
Attn: G. Grant

Badger Energy, Inc.
One Broadway
Cambridge, MA 02142
Attn: C. A. Bolthrunis

Bechtel Corporation (2)
P.O. Box 3965
San Francisco, CA 94119
Attn: E. Lam
R. Lessley

Black & Veatch Consulting Engineers (2)
P.O. Box 8405
Kansas City, MO 64114
Attn: J. E. Harder
J. C. Grosskreutz

Combustion Engineering, Inc.
1000 Prospect Hill Road
Windsor, Connecticut 06095
Attn: G. H. Rowe

EIC Laboratories, Inc.
55 Chapel Street
Newton, MA 02158
Attn: S. H. White

Electric Power Research Institute
P.O. Box 10412
3412 Hillview Avenue
Palo Alto, CA 94303
Attn: J. Bigger

Energy Concepts Co.
627 Ridgely
Annapolis, MD 21401
Attn: D. C. Ericksen

Foster Wheeler Development Corporation (4)
12 Peach Tree Hill Road
Livingston, NJ 07039
Attn: R. J. Zoschak
A. C. Gangadharan
W. Wolowodiuk
W. R. Apblett

Gas Cooled Reactor Association
3344 N. Torrey Pines Road
La Jolla, CA 92137
Attn: D. J. Spellman

General Atomic Company (2)
P.O. Box 81608
San Diego, CA 92138
Attn: T. H. VanHagen
J. L. Kaae

Jet Propulsion Laboratory (2)
4800 Oak Grove Drive
Pasadena, CA 91103
Attn: J. Becker
V. Truscello

Martin Marietta Corporation (2)
P.O. Box 179
Denver, CO 80201
Attn: T. R. Tracey
R. K. McMordie

McDonnell Douglas Astronautics Company (5)
5301 Bolsa Avenue
Huntington Beach, CA 92647
Attn: R. Easten
D. L. Endricott
L. Dreier
C. M. Finch
R. Riedesal

Oak Ridge National Laboratory
P.O. Box X
Oak Ridge, TN 37830
Attn: J. H. DeVan

Olin Corporation (2)
275 Winchester Avenue
New Haven, CT 06511
Attn: L. C. Fiorucci
S. L. Goldstein

Olin Corporation (2)
120 Long Ridge Road
Stamford, CT 06904
Attn: N. Christopher
R. E. Smith

Dr. Robert A. Ostergoung
Department of Chemistry
State University of New York at Buffalo
Buffalo, NY 14214

Pacific Gas and Electric Company (2)
Department of Engineering Research
3400 Crow Canyon Road
San Ramon, CA 94583
Attn: H. E. Seielstad
J. Raggio

Park Chemical Company
8074 Military Avenue
Detroit, MI 48204
Attn: R. W. Foreman

Public Service Company of New Mexico
P.O. Box 2267
Albuquerque, NM 87103
Attn: D. J. Groves

Rockwell International
Energy Systems Group
8900 De Soto Avenue
Canoga Park, CA 91304
Attn: T. S. Springer

Rockwell International
Rocketdyne Division
6633 Canoga Avenue
Canoga Park, CA 91304
Attn: J. M. Friefeld

Sierra Pacific Power Company
P.O. Box 10100
Reno, NV 89501
Attn: R. G. Richards

Solar Energy Research Institute (4)
1617 Cole Boulevard
Golden, CO 80401
Attn: B. Butler
B. P. Gupta
J. M. Lefferdo
SERI Library

Southern California Edison (2)
P.O. Box 800
Rosemead, CA 91770
Attn: J. N. Reeves
R. S. Williamson

Southwestern Public Service Company
P.O. Box 1261
Amarillo, TX 79170
Attn: K. Ladd

Solar Thermal Systems
Division of Exxon Enterprises, Inc.
P.O. Box 592
Florham Park, NJ 07932
Attn: P. Joy

Stearns-Roger Engineering Corporation
P.O. Box 58888
Denver, CO 80217
Attn: W. R. Lang

United Engineers and Construction
30 S. 17th Street
Philadelphia, PA 19103
Attn: A. Rosica

General Electric Company
3172 Porter Drive
Palo Alto, CA 94304
Attn: F. F. Witt

West Texas Utilities Company
P.O. Box 841
Abilene, TX 79604
Attn: R. R. Stanaland

A. Narath, 4000
J. H. Scott, 4700
D. G. Schueler, 4720
J. K. Galt, 5000
R. S. Claassen, 5800
M. J. Davis, 5830
R. W. Rohde, 5832
N. J. Magnani, 5840; Attn: R. B. Diegle, 5841
T. B. Cook, 8000; Attn: D. M. Olson, 8100
A. N. Blackwell, 8200
L. Gutierrez, 8400
D. M. Olson, 8120; Attn: R. J. Gallagher, 8124
B. F. Murphey, 8300
D. M. Schuster, 8310
D. A. Nissen, 8312
R. W. Mar, 8313
R. W. Bradshaw, 8313 (12)
A. S. Nagelberg, 8313
A. J. West, 8314
L. A. West, 8315
J. C. Swearengen, 8316
S. H. Goods, 8316
R. L. Rinne, 8320; Attn: C. F. Melius, 8326
G. W. Anderson, 8330
W. Bauer, 8340
R. C. Wayne, 8430
C. T. Yokomizo, 8451
A. C. Skinrood, 8452
W. G. Wilson, 8453
D. B. Dawson, 8453
Publications Division, 8265, for TIC (2)
Publications Division, 8264/Technical Library Processes Division, 3141
Technical Library Processes Division, 3141 (3)
M. A. Pound, 8214 for Central Technical Files (3)